10.24425/acs.2025.156306

Archives of Control Sciences
Volume 35(LXXI), 2025
No. 3*, pages 441–454*

Coupled 6DoF nonlinear model of tactical missiles: an optimal autopilot design

Tadeusz MIKUTEL, Sławomir STĘPIEŃ and Jan SYKULSKI

A fully coupled six degrees of freedom modelling of a tactical missile and an optimal control theory-based method are presented aiming at minimizing the autopilot control effort and improving the accuracy of reaching the target by a missile guidance system. A state-dependent Riccati equation-based regulator of controls deflection with an infinite time horizon is employed and its appropriateness for this type of a problem clarified. With the purpose of improving the precision of the autopilot system using a classic three-loop approach, a nonlinear state-dependent optimal feedback compensation with anti-windup system has been used incorporating measurements from an accelerometer and gyro rates. The simulated results for the missile model and optimal autopilot structure are compared with classic three-loop autopilot approach in a guidance system.

Key words: missile; autopilot; guidance; nonlinear optimal control

1. Introduction

The modern and precise tactical missiles exhibit unprecedented performance within a lightweight, cost-effective package. They use advanced systems of inertial guidance, optimized autopilots, fast sensors and an on-board active seeker-tracker system to find the intended target and complete the intercept [6,9]. Thanks to continuing development and ongoing modernization, they maintain their position as important combat weapons for air dominance [12, 14]. The precision of tactical missiles is enhanced by optimized flight control processors and algorithms; there is evidence of significant recent advances in transforming this

T. Mikutel and S. Stępień (corresponding author, e-mail: slawomir.stepien@itwl.pl) are with Air Force Institute of Technology, Księcia Bolesława 6, 01-494 Warsaw, Poland.

J. Sykulski is with University of Southampton, Southampton, SO17 1BJ, United Kingdom.

This research was partially funded by the National Centre for Research and Development in Poland, project no.: DOB-BIO-12-08-008-2023.

Received 14.03.2025. Revised 7.6.2025.

breakthrough concept into a practical high-precision missile system offering operational flexibility in air-to-air and surface-launch engagements, for example: AIM-120 AMRAAM (Advanced Medium-Range Air-to-Air Missile) [13], AGR-20A APKWS (Advanced Precision Kill Weapon Systems) [15] or Piorun LZR (Polish: Lotniczy Zestaw Rakietowy) currently under design by the Air Force Institute of Technology in cooperation with Mesko company [17].

The ongoing modernization of military forces and their battlefield use mean that accurate and precise control of guided missile systems continues to be an active area of research [3]. Efforts focus on finding solutions which ensure high immunity of the autopilot system to operational conditions, thus following prescribed trajectories while minimizing associated errors in guidance and reducing the miss distance [16]. The literature coverage in this field is immense, but some specific topics deserve a mention, in particular the use of an optimal control theory in optimized autopilot structures [1, 6, 8, 10]. The optimal State-Dependent Riccati Equation method (SDRE) – as an emerging control design methodology – has been used in [2, 4, 5, 7] to produce advanced guidance algorithms, in [14] for autopilot design, in [10] for a nonlinear benchmark problem design and is also briefly mentioned in [1, 14].

One of the best suited approaches to the optimal missile control involves using coupled 6DoF nonlinear modelling, which enables accurate determination of an autopilot cost function, a weighting on the acceleration error and the control rate allowing optimal control theory with an SDRE regulator to be employed [2,7]. The outcome is a new optimal structure autopilot for a tracking problem that allows to minimize the miss distance to the target. The nonlinear model of the missile and a new innovative optimal autopilot control system for flight stabilization are applied to the guidance system and compared with a commonly used autopilot structure. The miss distance to the target is tested and analyzed in a guidance system [9].

2. Nonlinear state-space missile model

When considering a typical missile and establishing the equations of motion according to Newton's laws, the rigid body equations of motion are differential equations that describe the evolution of basic states of an aircraft [3]. In deriving the rigid-body equations of motion, the following assumptions are made:

- the missile body is rigid, which means that the body does not undergo any change in size or shape,
- the missile is aerodynamically symmetric in roll, thus the aerodynamic forces and moments acting on the missile body are assumed to be invariant

with the roll position of the missile relative to the free-stream velocity vector,

- the missile mass is constant.

The missile position in global (operator) and local (body) frames is presented in Fig. 1.

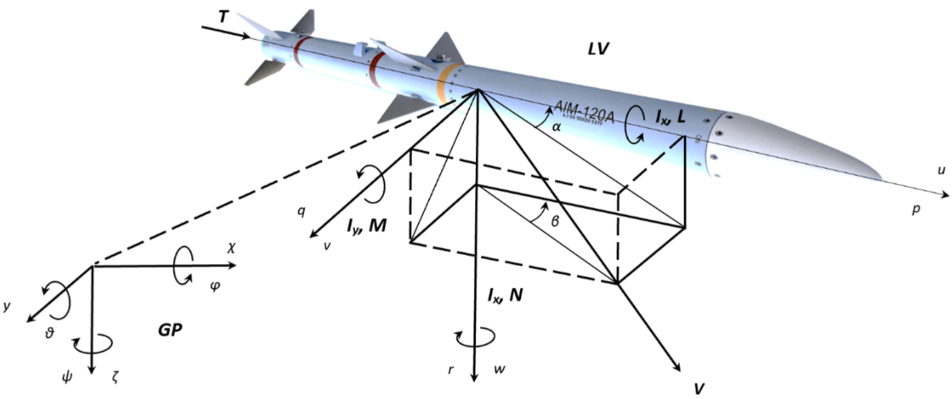

Figure 1: Missile linear and angular relationships [13]

By employing GP-LV (Global Position – Local Velocity) convention [11], the absolute linear position vector of a missile in the inertial frame (GP) is

$$\boldsymbol{\xi}_1 = \begin{bmatrix} x & y & z \end{bmatrix}^T, \tag{1}$$

where the three Euler angles in the inertial frame, i.e. the roll-pitch-yaw angles, are set in a vector

$$\boldsymbol{\xi}_2 = \begin{bmatrix} \varphi & \theta & \psi \end{bmatrix}^T. \tag{2}$$

The linear velocity vector in local body frame (LV) is

$$\boldsymbol{\upsilon}_1 = \begin{bmatrix} u & v & w \end{bmatrix}^T \tag{3}$$

and the angular velocity vector in the same frame is

$$\boldsymbol{\upsilon}_2 = \begin{bmatrix} p & q & r \end{bmatrix}^T. \tag{4}$$

The kinematic relationship between the inertial and body frame is as follows:

$$\dot{\boldsymbol{\xi}}_1 = \boldsymbol{R}_{zyx}(\boldsymbol{\xi}_2)\boldsymbol{\upsilon}_1, \tag{5}$$

where $\mathbf{R}_{zyx}(\boldsymbol{\xi}_2)$ is a rotation matrix around three axes of the inertial frame. Moreover, the kinematic relationship between angular velocities is the following:

$$\dot{\boldsymbol{\xi}}_2 = T(\boldsymbol{\xi}_2)\boldsymbol{\upsilon}_2, \tag{6}$$

where $\mathbf{T}(\boldsymbol{\xi}_2)$ transforms local velocities into the global ones, i.e. inertial.

Following from the above coordinate descriptions (1)–(4), the state vector of the missile model may be assembled in 6DOF as

$$x = \begin{bmatrix} \boldsymbol{\xi}_1^T & \boldsymbol{\xi}_2^T & \boldsymbol{\upsilon}_1^T & \boldsymbol{\upsilon}_2^T \end{bmatrix} = \begin{bmatrix} x & y & z & \varphi & \theta & \psi & u & v & w & p & q & r \end{bmatrix}^T. \tag{7}$$

Considering the missile space behavior, the six degrees of freedom consist of three translations and three rotations, along and about the missile axes (1). These motions are illustrated in Fig. 1, the translations being (3) and the rotations (4). In compact form, the translation and rotation of a rigid body may be expressed mathematically as:

$$\boldsymbol{F} = m\frac{\mathrm{d}}{\mathrm{d}t}\left(\dot{\boldsymbol{\xi}}_1\right) = m\dot{\boldsymbol{\upsilon}}_1 + m\left(\boldsymbol{\upsilon}_2 \times \boldsymbol{\upsilon}_1\right) \tag{8}$$

and

$$\boldsymbol{T} = \boldsymbol{r}_O \times \boldsymbol{F} = \boldsymbol{I}\dot{\boldsymbol{\upsilon}}_2 + \boldsymbol{\upsilon}_2 \times \boldsymbol{I}\boldsymbol{\upsilon}_2\,, \tag{9}$$

where $\boldsymbol{r}_O$ is the distance between the inertial and the body frame, m is the missile mass and $\boldsymbol{F}$ denotes the force vector, while $\boldsymbol{I}$ is the inertia matrix and $\boldsymbol{T}$ denotes the torque vector.

Based on the dynamic equations (8)–(9) and considering the missile state (7), the missile dynamics can be described in a coupled affine form with respect to the state-space notation [9]:

$$\begin{bmatrix} \dot{\boldsymbol{\xi}}_1 \\ \dot{\boldsymbol{\xi}}_2 \\ \dot{\boldsymbol{\upsilon}}_1 \\ \dot{\boldsymbol{\upsilon}}_2 \end{bmatrix} = \begin{bmatrix} \boldsymbol{R}_{zyx}\left(\boldsymbol{\xi}_2\right)\boldsymbol{\upsilon}_1 \\ \boldsymbol{T}\left(\boldsymbol{\xi}_1\right)\boldsymbol{\upsilon}_2 \\ \boldsymbol{C}_1\left(\boldsymbol{\upsilon}_2\right)\boldsymbol{\upsilon}_1 - \boldsymbol{M}^{-1}\boldsymbol{D}\left(\boldsymbol{\upsilon}_1\right) - \boldsymbol{M}^{-1}\boldsymbol{G}\left(\boldsymbol{\xi}_2\right) \\ \boldsymbol{I}^{-1}\boldsymbol{C}_2\left(\boldsymbol{\upsilon}_2\right)\boldsymbol{\upsilon}_1 + \boldsymbol{I}^{-1}\boldsymbol{C}_3\boldsymbol{\upsilon}_2 + \boldsymbol{I}^{-1}\boldsymbol{C}_4\left(\boldsymbol{\upsilon}_1\right) \end{bmatrix} + \begin{bmatrix} \boldsymbol{0} \\ \boldsymbol{0} \\ \boldsymbol{M}^{-1}\boldsymbol{B}_1 \\ \boldsymbol{I}^{-1}\boldsymbol{B}_2 \end{bmatrix}\boldsymbol{u}. \tag{10}$$

The fully coupled 6DOF missile model (10) includes terms related to Coriolis and centrifugal forces $\boldsymbol{C}_1\left(\boldsymbol{\upsilon}_2\right)\boldsymbol{\upsilon}_1$ and $\boldsymbol{C}_2\left(\boldsymbol{\upsilon}_2\right)\boldsymbol{\upsilon}_1$, respectively, gravity vector $\boldsymbol{G}(\boldsymbol{\xi}_2)$, drag matrix $\boldsymbol{D}\left(\boldsymbol{\upsilon}_1\right)$, matrix $\boldsymbol{C}_3$ related to missile angular velocity and vector $\boldsymbol{C}_4(\boldsymbol{\upsilon}_1)$ related to aerodynamic moments assumed to be functions of the Mach number (missile velocity) and nonlinear with the flow incidence angle. Matrices $\boldsymbol{B}_1$ and $\boldsymbol{B}_2$ are related to the control vector $\boldsymbol{u} = \begin{bmatrix} T & \delta_e & \delta_r \end{bmatrix}^T$, where T is a thrust and δ_e, δ_r are elevator and rudder deflections [6].

3. Classic longitudinal three-loop autopilot

The missile longitudinal autopilot controls acceleration normal to the missile body. In common implementations, the autopilot structure is a three-loop design that uses measurements from an accelerometer placed ahead of the center of gravity [10]. Additionally, the missile sensor system includes a gyroscope, where a rate gyro provides information about actual pitch speed. The controller gains are scheduled on missile incidence and speed number and are tuned for robust performance at the altitude of flight.

A typical Pitch Autopilot consists of a main accelerometer feedback loop to provide conversion of the commanded acceleration into the missile acceleration, and a velocity feedback loop that provides the necessary missile speed stabilization. In addition, to eliminate oscillations in the control system, an Anti-Windup loop is necessary.

Figure 2 shows three autopilot inputs: α – missile AoA (Angle of Attack) and M – missile Mach speed, q – pitching angular speed and e – acceleration error in z direction [9]:

$$e = a_{zc} - K(\alpha, M)a_{zm} . \tag{11}$$

Gains $K_1(\alpha, M)$, $K_2(\alpha, M)$ and $K_3(\alpha, M)$ are linear functions of α and Mach speed M. The Anti-Windup gain K_{AW} is assumed to be constant. The autopilot output δ_e is a signal prepared for a fin actuator as the missile elevator deflection.

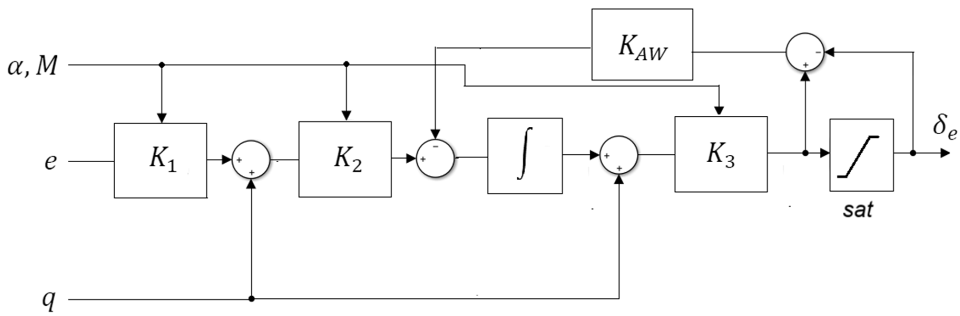

Figure 2: Classic three-loop autopilot structure

4. Optimal autopilot design

As described in [16], optimal autopilot structure has been proposed in literature. The tracking problem consists of finding optimal deflection of the missile elevation that minimizes the objective function expressed as a weighted sum of the square of the error between the measured acceleration and the command, along with the control usage.

In this section, a new approach with a simple autopilot state-space model and a feedback optimal compensator is proposed. When defining an acceleration error and pitching speed error

$$e_a = a_{zc} - K(\alpha, M)a_{zm} \qquad \text{and} \qquad e_q = -q_m , \tag{12}$$

the autopilot state-space approach based on a classic three-loop structure can be described as

$$\dot{\boldsymbol{x}}_e = \boldsymbol{B}_c \boldsymbol{e}, \tag{13}$$

where

$$\boldsymbol{B}_c = \begin{bmatrix} K_1(\alpha, M) K_2(\alpha, M) & -K_2(\alpha, M) \\ 0 & 1 \end{bmatrix}. \tag{14}$$

When considering an optimal feedback and defining the error vector $\boldsymbol{e} = \begin{bmatrix} e_a & e_q \end{bmatrix}^T$, the new input can be stated as non-optimized and optimized error

$$\boldsymbol{e}_o = \boldsymbol{e} + e_{\text{opt}} \,, \tag{15}$$

where optimized error is also a combination of optimal feedback gain $\boldsymbol{K}_{\text{opt}}$ and state $\boldsymbol{x}_e$

$$\boldsymbol{e}_{\text{opt}} = -\boldsymbol{P}^{-1} \boldsymbol{B}_c^T \boldsymbol{K}_{\text{opt}} \boldsymbol{x}_e \,. \tag{16}$$

By considering (13) and (15)–(16), the autopilot closed-loop form becomes

$$\dot{\boldsymbol{x}}_e = \boldsymbol{B}_c \boldsymbol{e}_o = \boldsymbol{B}_c \boldsymbol{e} - \boldsymbol{B}_c \boldsymbol{P}^{-1} \boldsymbol{B}_c^T \boldsymbol{K}_{\text{opt}} \boldsymbol{x}_e \,, \tag{17}$$

where the input $\boldsymbol{e}$ can be defined as a function of autopilot inputs

$$\boldsymbol{e} = \boldsymbol{B}_a \boldsymbol{u}, \tag{18}$$

where

$$\boldsymbol{B}_a = \begin{bmatrix} 1 & -K_1(\alpha, M) & 0 \\ 0 & 0 & -1 \end{bmatrix} \qquad \text{and} \qquad \boldsymbol{u} = \begin{bmatrix} a_{zc} & a_{zm} & q_m \end{bmatrix}^T. \tag{19}$$

Finally, the full closed-loop form is

$$\dot{\boldsymbol{x}}_e = \boldsymbol{B}_c \boldsymbol{e}_o = -\boldsymbol{B}_c \boldsymbol{P}^{-1} \boldsymbol{B}_c^T \boldsymbol{K}_{\text{opt}} \boldsymbol{x}_e + \boldsymbol{B}_c \boldsymbol{B}_a \boldsymbol{u} \tag{20}$$

with saturated output

$$\delta_e = \text{sat} \left\{ K_3(\alpha, M) \left(x_{ea} + x_{eq} \right) ; \ \pm 30^\circ \right\}. \tag{21}$$

To prevent integration wind-up in the autopilot controller, when the actuator is saturated, an anti-windup subsystem is introduced. This is helpful in situations such as controlling the fin actuator, where the actuator will have a maximum elevator deflection that must not be exceeded.

Thus the autopilot dynamics (Fig. 3) that includes anti-windup subsystem is

$$\begin{aligned} \dot{\boldsymbol{x}}_e = {} & -\boldsymbol{B}_c \boldsymbol{P}^{-1} \boldsymbol{B}_c^T \boldsymbol{K}_{\text{opt}} \boldsymbol{x}_e + \boldsymbol{B}_c \boldsymbol{B}_a \boldsymbol{u} \\ & - K_{\text{AW}} \begin{bmatrix} K_3(\alpha, M) \left(x_{ea} + x_{eq} \right) \\ -\text{sat} \left\{ K_3(\alpha, M) \left(x_{ea} + x_{eq} \right) ; \ \pm 30^\circ \right\} \end{bmatrix}. \end{aligned} \tag{22}$$

The model (22) is nonlinear because matrices $\boldsymbol{B}_c$ and $\boldsymbol{B}_a$ depend on angle α and Mach speed M. Therefore, the optimal feedback gain can be obtained using optimal control techniques such State-Dependent Riccati Equation method (SDRE) for nonlinear systems [2, 4, 5, 7].

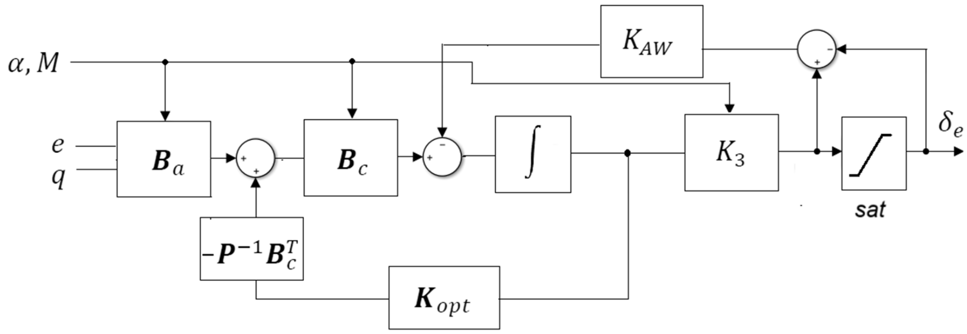

Figure 3: Optimal autopilot structure

5. Optimal tracking solution

When considering the tracking problem, an obvious optimization objective [2] would be to use a weighted sum of the square of the error between the measured acceleration and the command, along with the control usage. The following objective function is minimized for H_∞ problem [4]:

$$J(\boldsymbol{u}) = \frac{1}{2}\int_0^\infty \left(\boldsymbol{x}_e^T \boldsymbol{Q} \boldsymbol{x}_e + \boldsymbol{e}_{\text{opt}}^T \boldsymbol{P} \boldsymbol{e}_{\text{opt}}\right) \mathrm{d}t, \tag{23}$$

subject to nonlinear autopilot dynamics for affine systems

$$\dot{\boldsymbol{x}}_e = \boldsymbol{B}_c(\boldsymbol{x}_e)\boldsymbol{e}_{\text{opt}} \,. \tag{24}$$

By employing the optimal control theory, the solution results in a control law (16). To obtain $\boldsymbol{K}_{\text{opt}}(\boldsymbol{x}_e)$, which is the nonlinear optimal gain, it is assumed that $\boldsymbol{K}_{\text{opt}}(\boldsymbol{x}_e)$ is the suboptimal solution to

$$\begin{aligned}\boldsymbol{K}_{\text{opt}}(\boldsymbol{x}_e)\boldsymbol{A}_c(\boldsymbol{x}_e) + \boldsymbol{A}_c(\boldsymbol{x}_e)^T\boldsymbol{K}_{\text{opt}}(\boldsymbol{x}_e)\\ - \boldsymbol{K}_{\text{opt}}(\boldsymbol{x}_e)\boldsymbol{B}_c(\boldsymbol{x}_e)\boldsymbol{P}^{-1}\boldsymbol{B}_c(\boldsymbol{x}_e)^T\boldsymbol{K}_{\text{opt}}(\boldsymbol{x}_e) + \boldsymbol{Q} = \boldsymbol{0},\end{aligned} \tag{25}$$

where $\boldsymbol{A}_c(\boldsymbol{x}_e) = \boldsymbol{0}$ in this case.

6. Control system analysis

The nonlinear missile model is applied to validate the described optimal autopilot equipped with the infinite-time SDRE control for a longitudinal tracking problem when the required acceleration given by the guidance system must be obtained. The missile-autopilot model consists of four principal subsystems, controlled through the acceleration-demand autopilot [16] as shown in Fig. 4.

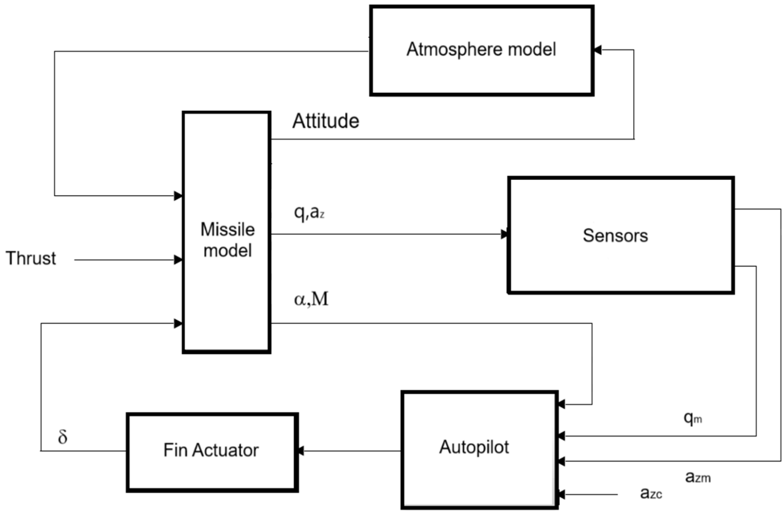

Figure 4: Missile-autopilot control system structure

The Atmosphere subsystem calculates the change in atmospheric conditions in stratosphere and troposphere regions with changing altitude. The Fin Actuator and Sensors subsystems couple the autopilot to the airframe. The Missile model subsystem calculates the magnitude of the forces and moments acting on the missile body with constant thrust and integrates the equations of motion.

The missile model parameters are presented in Table 1.

Table 1: Missile model parameters

Parameter	Value [quantity]
m	204.0227 kg
I_y	247.4366 kg·m^2

The autopilot parameters are presented in Table 2. Parameters for both the classic and the optimal case are generally the same, but the optimal is enhanced by an additional feedback compensator, whose parameters are computed from Eq. (25) for $\boldsymbol{Q} = 0.01 \cdot \boldsymbol{I}_{2\times2}$ and $\boldsymbol{P} = \boldsymbol{I}_{2\times2}$, where $\boldsymbol{I}_{2\times2}$ is the 2×2 identity matrix.

Table 2: Classis and optimal autopilot parameters

Parameters	Value [quantity
$K(\alpha, M)$	$0.28\lvert\alpha\rvert + 0.3M$
$K_1(\alpha, M)$	$0.0025\lvert\alpha\rvert + 0.025M$
$K_2(\alpha, M)$	$20\lvert\alpha\rvert + 50M$
$K_3(\alpha, M)$	$0.025\lvert\alpha\rvert + 0.225M$

First, the aim is to check the missile-autopilot control system step response (without the guidance system) when prescribed acceleration $a_{zc} = -10g$ is applied.

Figures 5a and 5b show expected and achieved normal acceleration in both cases. As can be seen, the optimal feedback compensator (optimal autopilot

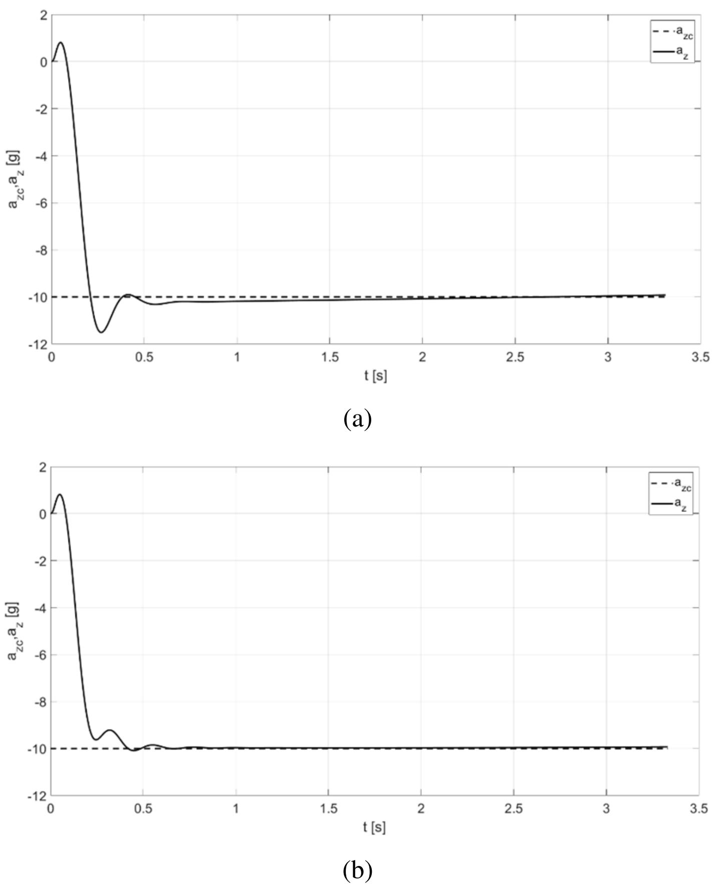

(a)

(b)

Figure 5: (a) The step response for classic autopilot case;
(b) The step response for optimal autopilot case

variant) significantly reduces the overshoots, eliminates the steady state error and makes the control process faster.

Both variants of the autopilot are applied to the guidance system [9, 16], employing the strongly coupled 6DoF missile model described in Section 2. The full guidance system structure is presented in Fig. 6.

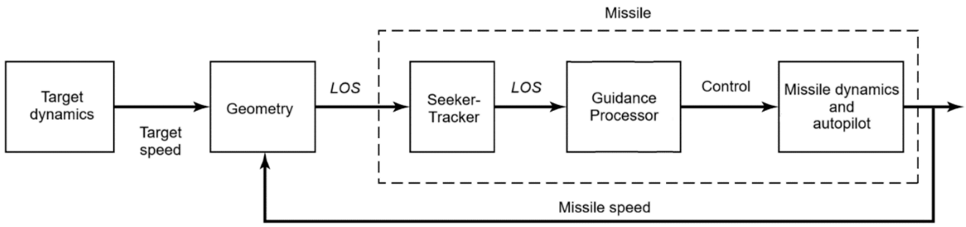

Figure 6: Guidance system structure

The Guidance Processor generates demands during the closed-loop tracking and performs an initial search to locate the target position. Once the seeker has acquired the target using the line-of-sight (LOS), a proportional navigation guidance (PNG) law is used to guide the missile until impact [14].

As an example, the model of the missile airframe presented above has been used in advanced control methods applied to the missile optimal autopilot design. The example represents a tail-controlled missile traveling between 2–4 Mach speed, at altitudes ranging between 3–20 km, with typical angles of attack (AoA) ranging between ±20 degrees [16]. The results are presented and compared for the classic three-loop autopilot structure and the optimized structure. The missile is powered by a constant thrust 10 kN. A missile and target trajectory are presented in Fig. 7a. The fins control effort, i.e. fins deflection, is presented in Fig. 7b.

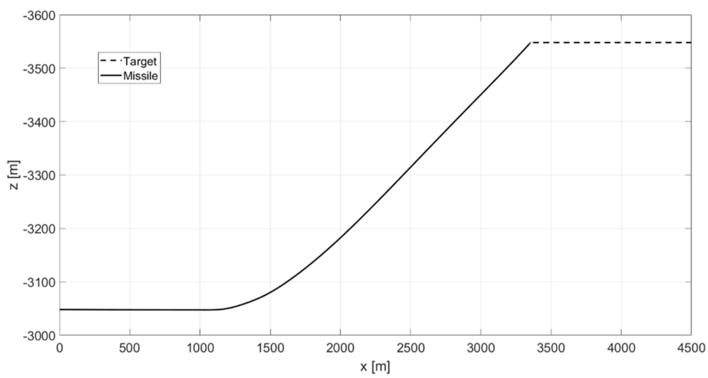

(a)

Figure 7

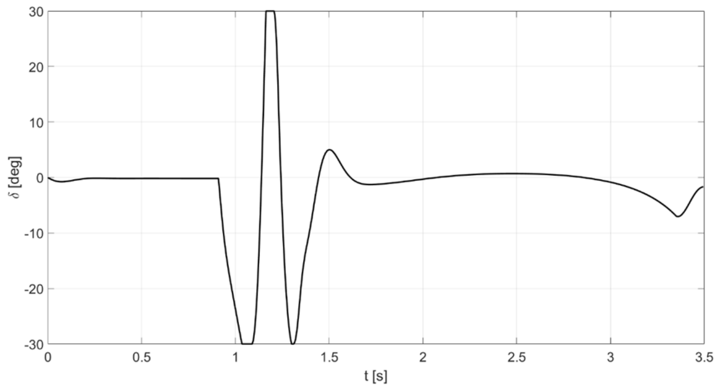

(b)

Figure 7: (a) Missile and target trajectory – classic autopilot; (b) Fins deflection – classic autopilot

Finally, to show the missile trajectory and fins effort when optimal autopilot structure is applied, the trajectory is presented in Fig. 8a and fins deflection in Fig. 8b.

When looking at Figs. 7a and 8a, the missile trajectories appear to be the same. Indeed, they are similar, but the difference is visible in the context of target kill precision when the intercept is completed. For the classic autopilot approach the miss distance to target is 0.167 m, but for the optimal one it is reduced by about 50%. As the detonate algorithm depends on the intercept precision, thus the missile can detonate the load more closely to the target. The difference between the missile guidance systems is more visible in Figs. 7b and 8b. The missile is more precisely stabilized by the optimal feedback control, although the effort of the autopilot controller is slightly bigger to achieve the improved precision. The efficiency of the control system has an impact on the missile-target miss distance, as demonstrated in Table 3.

Table 3: Miss distance comparison

Autopilot structure	Value
Look-up-Table [16]	0.268 m
Classic	0.167 m
Optimal	0.077 m

From the results presented in Table 3, it is clear that the optimal autopilot is more precise.

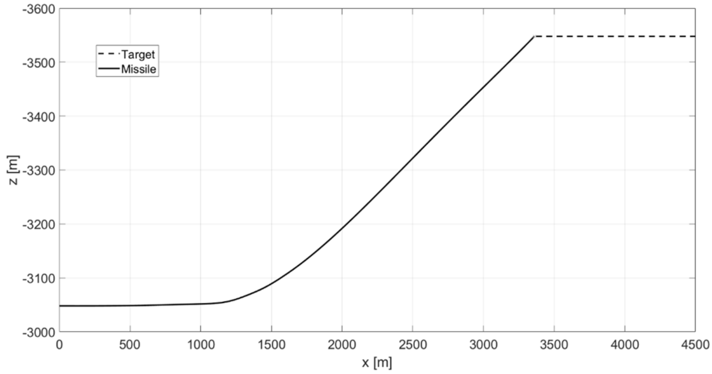

(a)

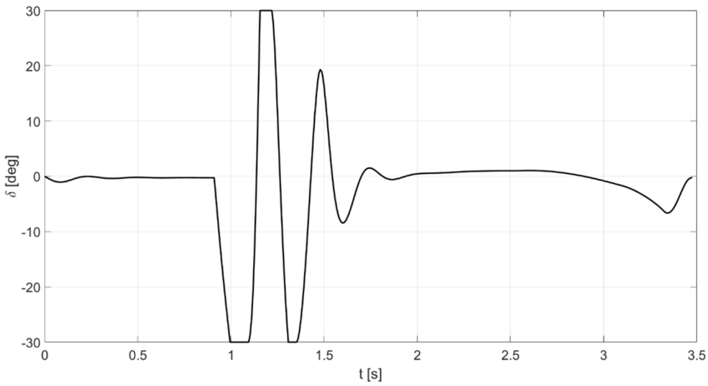

(b)

Figure 8: (a) Missile and target trajectory – optimal autopilot; (b) Fins deflection – optimal autopilot

7. Conclusions

The paper has proposed and completed the missile autopilot design by solving an optimal control problem for nonlinear systems. The optimal control technique has been applied and analyzed using the nonlinear feedback compensator for computation of the control input that minimizes the quadratic objective function, thus performing a stabilization task. The results are compared with the classic three-loop autopilot topology as well as those reported in literature. The effectiveness of the proposed technique is demonstrated using a numerical example where optimal missile controls are found for prescribed acceleration. Moreover, the proposed GP-LV missile model and the optimized autopilot structure have been applied in the missile guidance system. The presented results suggest that the proposed SDRE-based autopilot provides better accuracy in terms of the miss distance criterion. Interestingly, it appears that autopilot designers – who decades ago used the classic three-loop approach – already knew that this was a good topology to be used in missile guidance industry. However, today's challenge is to design and build new control systems employing optimal SDRE techniques for advanced autopilots and guidance processors to increase accuracy.

References

[1] R.J. Adams and N.M. Conrardy: *Design Plant Manipulations for Implementation of an LQR Controller in a Classical Three Loop Autopilot*. Technical report, Raytheon Missile Systems, 2003.

[2] H.T. Banks, B.M. Lewis and H.T. Tran: Nonlinear feedback controllers and compensators: a state-dependent Riccati equation approach. *Computational Optimization and Applications*, **37**(2), (2007), 177–218. DOI: 10.1007/s10589-007-9015-2

[3] A. Benaouali and S. Kachel: Multidisciplinary design optimization of aircraft wing using commercial software integration. *Aerospace Science and Technology*, **92** (2019), 766–776, DOI: 10.1016/j.ast.2019.06.040

[4] T. Çimen: Systematic and effective design of nonlinear feedback controllers via the state-dependent Riccati equation (SDRE) method. *Annual Reviews in Control*, **34**(1), (2010), 32–51. DOI: 10.1016/j.arcontrol.2010.03.001

[5] J.R. Cloutier, C.N. D'Souza and C.P. Mracek: Nonlinear regulation and nonlinear H∞ control via the state-dependent Riccati equation technique: Part 1, Theory; Part 2, Examples. In: *Proceedings of the First International Conference on Nonlinear Problems in Aviation and Aerospace*, Daytona Beach, FL, (1996), 117–141.

[6] F.A. Faruqi and T L. Vu: *Mathematical Models for a Missile Autopilot Design*. DSTO-TN-0449, DSTO Systems Sciences Laboratory, Edinburgh, South Australia, 2002. Available: https://apps.dtic.mil/sti/tr/pdf/ADA407845.pdf

[7] A. Heydari and S.N. Balakrishnan: Closed-form solution to finite-horizon suboptimal control of nonlinear systems. *International Journal of Robust and Nonlinear Control*, **25**(15), (2015), 2687–2704. DOI: 10.1002/rnc.3222

[8] K. Lu and Y. Xia: Finite-time fault-tolerant control for rigid spacecraft with actuator saturations. *IET Control Theory and Applications*, **7**(11), (2013), 1529–1539. DOI: 10.1049/iet-cta.2012.1031

[9] T. Mikutel, M. Pietraszek and S. Stepien: GP-LV missile model: Application in design of guidance systems. *Journal of KONBiN*, **54**(4) (2024), 45–68. DOI: 10.5604/01.3001.0054.9222

[10] C.P. Mracek and D.B. Ridgely: Missile longitudinal autopilots: Connections between optimal control and classical topologies. *AIAA Guidance, Navigation, and Control Conference and Exhibit*, San Francisco CA, (2005). DOI: 10.2514/6.2005-6381

[11] S.R. Nekoo, J.Á. Acosta and A. Ollero: Fully coupled six-DoF nonlinear suboptimal control of a quadrotor: Application to variable-pitch rotor design. In: M. Silva, J.L. Lima, L. Reis, A. Sanfeliu and D. Tardioli (Eds): *Robot 2019: Fourth Iberian Robotics Conference.*

ROBOT 2019. Advances in Intelligent Systems and Computing, (2020), 1093. Springer, Cham. DOI: 10.1007/978-3-030-36150-1_7

[12] A. Olejnik, S. Kachel, P. Zalewski, R. Rogólski, M. Jędrak and M. Szcześniak: Finite element analysis of the underslung carrier rocket effect on stress and strain distribution in a structure of the MiG-29 aircraft. *Proceedings of the Institution of Mechanical Engineers, Part G: Journal of Aerospace Engineering*, **237**(14), (2023), 3285–3303. DOI: 10.1177/09544100231189942

[13] J.A. Tirpak: Raytheon: AMRAAM and JATM missiles 'complementary' for future force mix. *Air & Space Forces Magazine*, (2024).

[14] P. Zarchan: *Tactical and Strategic Missile Guidance*. Fourth Edition. AIAA Volume 199, Progress in Astronautics and Aeronautics, Reston, VA, 2002.

[15] APKWS Upgrade Extends Range By 30 Percent: BAE. Breaking Defense. 3 August 2021. Available: https://breakingdefense.com/2021/08/apkws-upgrade-extends-range-by-30-percent-bae/

[16] Design a Guidance System in MATLAB and Simulink, Documentation, Available: www.mathworks.com/help/simulink/slref/designing-a-guidance-system-in-matlab-and-simulink.html

[17] Lotniczy Zestaw Rakietowy Piorun od ITWL. Available: https://milmag.pl/mspo-2022-lotniczy-zestaw-rakietowy-piorun-od-itwl/ (in Polish).